

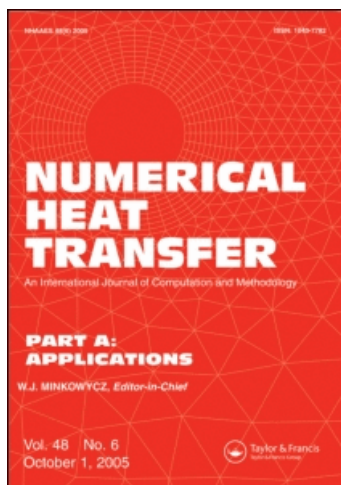
This article was downloaded by: [China Science & Technology University]

On: 11 November 2008

Access details: Access Details: [subscription number 788829259]

Publisher Taylor & Francis

Informa Ltd Registered in England and Wales Registered Number: 1072954 Registered office: Mortimer House, 37-41 Mortimer Street, London W1T 3JH, UK



## Numerical Heat Transfer, Part A: Applications

Publication details, including instructions for authors and subscription information:

<http://www.informaworld.com/smpp/title-content=t713657973>

### Numerical Study of Convective Heat Transfer from Two Identical Square Cylinders Submerged in a Uniform Cross Flow

Jianlei Niu <sup>a</sup>; Zuojin Zhu <sup>b</sup>; Shenghong Huang <sup>c</sup>

<sup>a</sup> Department of Building Services Engineering, The Hong Kong Polytechnic University, Kowloon, Hong Kong, People's Republic of China <sup>b</sup> Department of Thermal Science and Energy Engineering, University of Science and Technology of China, Hefei, People's Republic of China <sup>c</sup> Department of Modern Mechanics, University of Science and Technology of China, Hefei, People's Republic of China

Online Publication Date: 01 February 2006

**To cite this Article** Niu, Jianlei, Zhu, Zuojin and Huang, Shenghong(2006)'Numerical Study of Convective Heat Transfer from Two Identical Square Cylinders Submerged in a Uniform Cross Flow', Numerical Heat Transfer, Part A: Applications, 50:1, 21 — 44

**To link to this Article:** DOI: 10.1080/10407780500496547

**URL:** <http://dx.doi.org/10.1080/10407780500496547>

PLEASE SCROLL DOWN FOR ARTICLE

Full terms and conditions of use: <http://www.informaworld.com/terms-and-conditions-of-access.pdf>

This article may be used for research, teaching and private study purposes. Any substantial or systematic reproduction, re-distribution, re-selling, loan or sub-licensing, systematic supply or distribution in any form to anyone is expressly forbidden.

The publisher does not give any warranty express or implied or make any representation that the contents will be complete or accurate or up to date. The accuracy of any instructions, formulae and drug doses should be independently verified with primary sources. The publisher shall not be liable for any loss, actions, claims, proceedings, demand or costs or damages whatsoever or howsoever caused arising directly or indirectly in connection with or arising out of the use of this material.

## NUMERICAL STUDY OF CONVECTIVE HEAT TRANSFER FROM TWO IDENTICAL SQUARE CYLINDERS SUBMERGED IN A UNIFORM CROSS FLOW

**Jianlei Niu**

*Department of Building Services Engineering, The Hong Kong Polytechnic University, Kowloon, Hong Kong, People's Republic of China*

**Zuojin Zhu**

*Department of Thermal Science and Energy Engineering, University of Science and Technology of China, Hefei, People's Republic of China*

**Shenghong Huang**

*Department of Modern Mechanics, University of Science and Technology of China, Hefei, People's Republic of China*

*This article presents numerical results of convective heat transfer from two identical square cylinders (TISC) arranged at close proximity in a uniform cross flow of air ( $Pr = 0.71$ ) at the particular Reynolds number of 250. The proximity arrangement of the TISC is defined by longitudinal spacing ranging from zero to unity, with the transverse spacing ranging from 0.125 to unity. Results are obtained by the finite-difference method for 25 cases, divided into five groups for convenience of discussion. It is found that the time-averaged or mean convective heat transfer rates from the TISC reach their maxima when the transverse spacing value is about 0.3 from the view of the group averaging at a given transverse spacing. The heat transfer rates from inner faces of the TISC are generally greater than those of the outer sides, by a factor of about 2 to 3. Depending on the TISC arrangement, a bifurcation sometimes occurs, with the bifurcated lower  $St$  value corresponding to the shedding from the outer shear layer, and the higher one corresponding to the shedding from the inner shear layer. The significant effect of the TISC arrangement on the flow-induced forces is also reported and discussed.*

### 1. INTRODUCTION

Convective heat transfer from square cylinders (SC) has important implications in thermal and building services engineering. For instance, with regard to the use of natural ventilation and concern about virus-laden aerosol spreading near

Received 22 July 2005; accepted 27 September 2005.

This work has been financially supported by Hong Kong RGC with Grants Polyu5031/01E and the Polyu-BSE project G-YC34.

Address correspondence to Jianlei Niu, Department of Building Services Engineering, FCLU, The Hong Kong Polytechnic University, Hungghom, Kowloon, Hong Kong, SAR, People's Republic of China. E-mail: Bejlniu@polyu.edu.hk

## NOMENCLATURE

<p><math>A, B</math> coefficients used in the third-order finite-difference scheme</p> <p><math>C_p</math> Specific heat of fluid</p> <p>CD coefficient of drag, defined by <math>FD/(0.5 u_{in}^2 d)</math></p> <p>CL coefficient of lift, defined by <math>FL/(0.5 u_{in}^2 d)</math></p> <p><math>d</math> side length of square cylinder, m</p> <p><math>f</math> vortex shedding frequency from the shear layers of the square cylinder, <math>s^{-1}</math></p> <p>FD total force per unit length in the longitudinal direction, N/m</p> <p>FL total force per unit length in the transverse direction, N/m</p> <p><math>H_x</math> length of the computational domain, m</p> <p><math>H_y</math> width of the computational domain, m</p> <p><math>L</math> longitudinal spacing, m</p> <p><math>Nu_{bf}</math> Nusselt number on the bottom face of the square cylinder, defined by <math>\int_0^1 \partial\Theta/\partial y dx</math> with <math>x, y</math> measured by the side length of the square cylinder</p> <p><math>Nu_{ff}</math> Nusselt number on the bottom face of the square cylinder, defined by <math>\int_0^1 \partial\Theta/\partial x dy</math> with <math>x, y</math> measured by the side length of the square cylinder</p> <p><math>Nu_m</math> Nusselt number for the square cylinder, defined by <math>(Nu_{bf} + Nu_{ff} + Nu_{tf} + Nu_{tr})/4</math></p>	<p><math>Nu_{rf}</math> Nusselt number on the top face of the square cylinder, defined by <math>-\int_0^1 \partial\Theta/\partial x dy</math> with <math>x, y</math> measured by the side length of the square cylinder</p> <p><math>Nu_{tr}</math> Nusselt number on the top face of the square cylinder, defined by <math>-\int_0^1 \partial\Theta/\partial y dx</math> with <math>x, y</math> measured by the side length of the square cylinder</p> <p>Pr Prandtl number (<math>=\alpha/\nu</math>)</p> <p>Re Reynolds number (<math>=du_{in}/\nu</math>)</p> <p>St Strouhal number, defined by <math>fd/u_{in}</math></p> <p><math>T</math> transverse spacing, m</p> <p><math>u</math> streamwise velocity component, m/s</p> <p><math>v</math> cross-stream velocity component, m/s</p> <p><math>x</math> Cartesian coordinate in the streamwise direction</p> <p><math>y</math> Cartesian coordinate in the spanwise direction</p> <p><math>\alpha</math> thermal diffusivity, <math>m^2/s</math></p> <p><math>\Theta</math> normalized temperature</p> <p><math>\nu</math> kinematic viscosity of fluid, <math>m^2/s</math></p> <p><math>\rho</math> fluid density, <math>kg/m^3</math></p> <p><b>Subscripts</b></p> <p><math>m</math> time average</p> <p><math>w</math> cylinder wall</p> <p>I bottom square cylinder</p> <p>II top square cylinder</p>
---	--

buildings [1], an accurate prediction of the heat transfer from square cylinders is essential for the assessment of the convective and diffusive transportation of passive scalars such as heat and the harmful aerosols around buildings.

Earlier experiments have provided empirical expressions for the convective heat transfer from a square cylinder at Reynolds numbers in the subcritical range [2–4]. Recent experiments have emphasized the response of vortex shedding behavior on the oncoming flow incidence and the bluff body shape changes [5–7]. The characteristics of square cylinder wake transition flows have been explored by using dye- and laser-induced fluorescence visualization [8]. It was found that the critical Reynolds numbers at which secondary flow modes occur for square cylinder flows were estimated to be approximately 160 and 200, respectively, and are lower than those found in circular cylinder flows, which are generally agreed to be approximately 188–190 and 230–260, respectively.

More extensive numerical work has been conducted for the flows around a bluff body [9–13]. For flow past a single square cylinder submerged in a uniform cross flow, it was found that the flow transition from two to three dimensionality occurs at a Reynolds number of 180 [10, 11].

The unsteady flow and heat transfer characteristics from square cylinders located in a channel with fully developed inlet velocity profile have been studied numerically by Rosales et al. [12, 13]. It was shown that the Nusselt number decreases for both a single and a tandem pair of cylinders as they approach the channel wall. The highest Strouhal number occurs in the channel-centered, inline-eddy configuration.

Using a control-volume finite-element method adapted to the staggered grid to solve the the complete Navier-Stokes and energy equations, Turki et al. [14] have studied the two-dimensional laminar air flow and heat transfer in a channel with a built-in heated square cylinder for Reynolds number ranging from 62 to 200 and Richardson number in the range from 0 to 0.1 when the blockage ratio was set as 25% or 12.5%. The results showed that the degeneration of the Karman vortex street, previously observed experimentally for the circular cylinder, also occurs for the more bluff square cylinder at a critical Richardson number of 0.15.

Sharma and Eswaran [15–17] have investigated numerically the heat and fluid flow across a square cylinder in the laminar regime, focusing on the effect of aiding and opposing buoyancy, the flow blockage ratio, and the channel confinement. Yang and Farouk [18] have studied the two-dimensional laminar mixed-convection flows around a heated horizontal square cylinder rotating slowly within a concentric circular enclosure, highlighting the detailed influence of the rotating noncircular geometry of the inner cylinder on the flow field and the heat transfer characteristics. The three-dimensional conjugate heat transfer in a rectangular duct with two discrete flush-mounted heat sources has been studied numerically by Wang and Jaluria [19], with particular interest paid to the transverse variation in the flow, temperature and heat transfer, the interaction between the heat sources, and the effects of conjugate transport.

The objective of this numerical study is to investigate the heat transfer from two identical square cylinders submerged in a steady cross flow, focusing on dependence on the proximity arrangement of the flow-induced forces and the convective heat transfer rates from the overall face of the square cylinders and each cylinder face, as well as the oscillating characteristic of the heat transfer process caused by the large-scale vortex shedding from the shear layers of the SC.

The remainder of this article is organized as follows: Section 2 gives the governing equations and the numerical methods, accompanied by assessment of the method with respect to earlier published results. Section 3 presents the results and discussion, where the flow-induced forces, Nusselt numbers, and the vorticity and temperature fields are presented. Conclusions are presented in Section 4.

## 2. GOVERNING EQUATIONS AND NUMERICAL METHOD

### 2.1. Governing Equations

As shown schematically in Figure 1, the square cylinder has a uniform surface temperature which is higher than that of the steady oncoming flow. The incident angle is set as zero. It is convenient to present equations in nondimensional variables. Choose the units

$$[l] = d \quad [t] = d/u_{in} \quad [\theta] = \theta_w - \theta_{in} \quad (1)$$

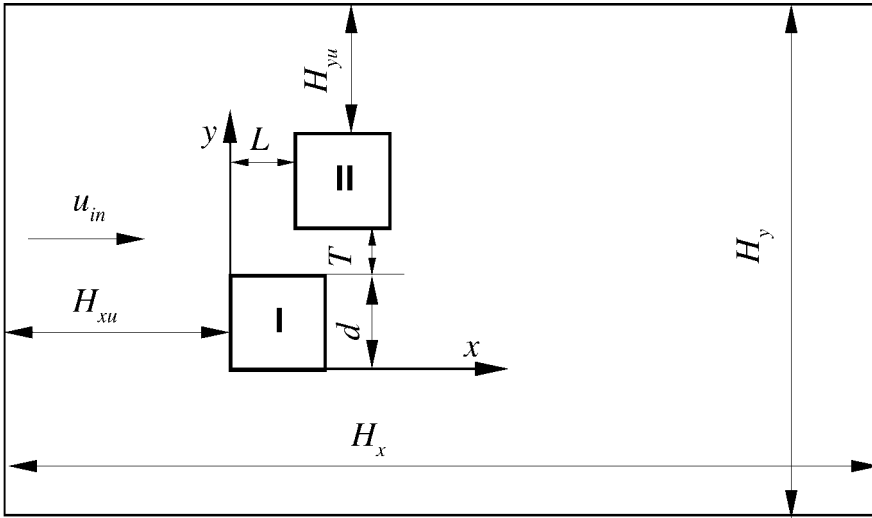


**Figure 1.** Schematic of flow past two identical square cylinders. Note that the transverse spacing is denoted as  $T$ , with longitudinal spacing given by  $L$ . The bottom square cylinder (SC I) has a distance of  $H_{xu}$  from the front face to the inlet bound of the computational domain, while the top square cylinder (SC II) has a distance of  $H_{yu}$  from the top face to the top bound of the computational domain. The two SC are arranged symmetrically to the horizontal centerline of the computational domain, with  $H_x$  and  $H_y$  representing the relevant length and width.

where  $u_{in}$  is the oncoming flow velocity and  $d$  is the side length of the square cylinder. The Reynolds number of the problem considered is  $Re = du_{in}/\nu$ , with  $\nu$  being the kinematic viscosity of the fluid;  $\theta_w$  and  $\theta_{in}$  are, respectively, the surface temperature of the SC and the temperature of the oncoming fluid. Representing the normalized temperature as  $\Theta = (\theta - \theta_{in})/[\theta]$ , the governing equation in a two-dimensional Cartesian coordinate system  $(x, y)$  can be written as

$$u_x + v_y = 0 \quad (2)$$

$$u_t + uu_x + vv_y = -p_x + \nabla^2 u / Re \quad (3)$$

$$v_t + uv_x + vv_y = -p_y + \nabla^2 v / Re \quad (4)$$

$$\Theta_t + u\Theta_x + v\Theta_y = \nabla^2 \Theta / Re Pr \quad (5)$$

where  $Pr (= \nu/\alpha)$  is the Prandtl number of the fluid, with the thermal diffusivity of the fluid denoted by  $\alpha$ . The corresponding vector form of the Navier-Stokes equations is given by

$$\nabla \cdot \mathbf{u} = 0 \quad (6)$$

$$\mathbf{u}_t + (\mathbf{u} \cdot \nabla) \mathbf{u} = -\nabla p + \nabla^2 \mathbf{u} / Re \quad (7)$$

The solutions of the governing equations (2)–(5) should be sought under appropriate boundary and initial conditions. For the boundary conditions (BC) on the square

cylinder walls, we have nonslip BC,

$$u = 0 \quad v = 0 \quad \Theta = 1 \quad (8)$$

while for the BC at the outlet, similar to the treatment utilized by Sohankar et al. [11] and Saha et al. [10], we use the Orlanski [20] type,

$$u_t + u_c u_x = 0 \quad v_t + u_c v_x = 0 \quad \Theta_t + u_c \Theta_x = 0 \quad (9)$$

With regard to the nondimensional form, we choose  $u_c = 1$ . At the inlet section, we have

$$u = 1 \quad v = 0 \quad \Theta = 0 \quad (10)$$

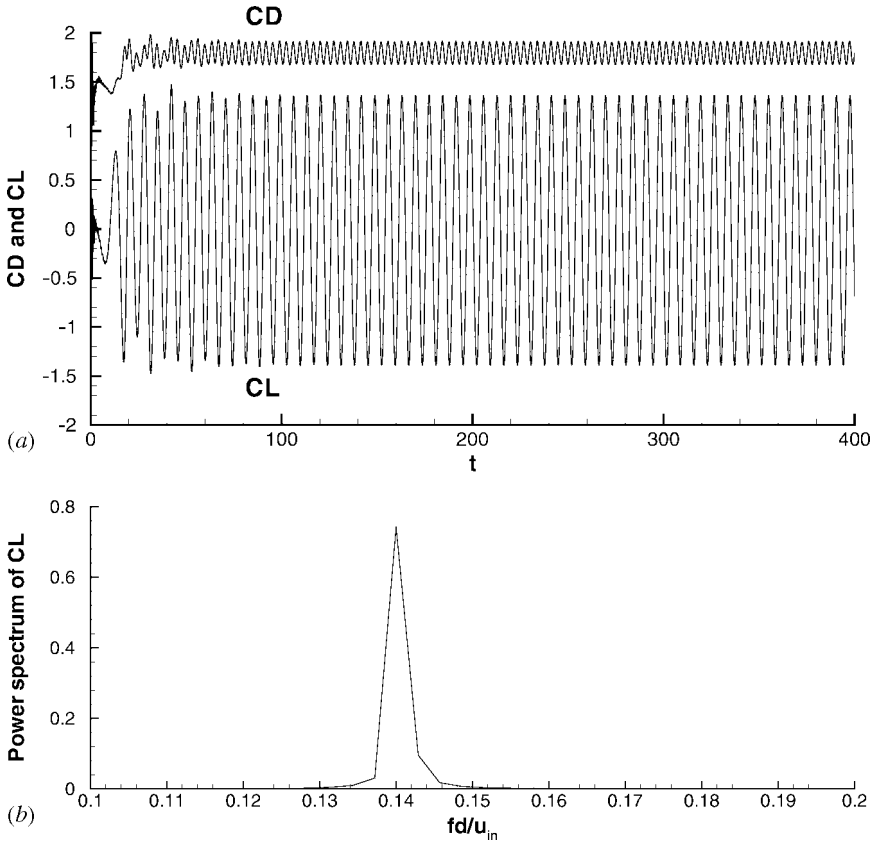


**Figure 2.** (a) Transient CD and CL for the flow past a single SC at a blockage of 5.56%. (b) Power spectrum of CL versus frequency. Note that the transient flow-induced forces were obtained by using the third-order upwind scheme for the discretization of convective terms in the Navier-Stokes equations, the grid number was  $181 \times 121$ , the time step scaled by  $(d/u_m)$  was 0.005, and the  $d$ -scaled distance from the rear face of the SC to the exit bound of the computational domain was set as 15. The results suggest a St of 0.140, a time-averaged CD value of 1.79, with the RMS values of CL and CD given by 0.969 and 0.081.

However, on the side boundary of the computational domain, we use

$$u_y = 0 \quad v = 0 \quad \Theta_y = 0 \quad (11)$$

The initial condition is given by

$$u = 1 \quad v = 0 \quad \Theta = 0 \quad (12)$$

## 2.2. Solution Method

The solutions for the convective heat transfer from two identical square cylinders (TISC) arranged in proximity region ( $T \in [0.125, 1.0]$ ,  $L \in [0, 1.0]$ ) are sought by using the accurate projection algorithm PmIII developed by Brown et al. [21]. The intermediate velocity components are calculated excluding the pressure gradient terms. The pressure Poisson equation is first solved by the approximate factorization one (AF1) scheme given by Baker [22], with the solution accuracy of pressure prediction improved by the stabilized bi-conjugate gradient method (Bi-CGSTAB) developed by Von der Vorst [23]. The convective terms in the Navier-Stokes equations are spatially differenced by a third-order upwind scheme, with the viscous diffusion terms treated by a second-order central difference scheme.

For example, the third-order upwind scheme treats the convective term  $uu_x$  in a staggered grid system in the following way:

$$(uu_x)_{ij} = u_{ij}[-(A + B + C)u_{ij} + Au_{i-1,j} + Bu_{i-2,j} + Cu_{i+1,j}] - Du_{ij}(u_{xxx})_{ij} \quad (13)$$

where the velocity component ( $u_{ij}$ ) is located at point  $(x_{i-1/2}, y_j)$ . The term including the fourth-order derivative of  $u$  in the above equation has to be used to remove the artificial viscous term from the Taylor expansion of terms with coefficients  $A$ ,  $B$ , and  $C$ . Our numerical experiments revealed that this upwind scheme is stable. Denoting that  $h_i = x_{i-1/2} - x_{i-1/2-1}$ , according to the Taylor expansion of the velocities at point  $(i-1, j)$ ,  $(i-2, j)$ , and  $(i+1, j)$ , Taylor expansion gives rise to the following

**Table 1.** Grid-independent inspection of numerical results of flow past the TISC for the case of  $Re = 250$  and  $T = L = 0.5$

For SC I							
Grid	$\Delta t \times 10^3$	CD	RMS of CD	CL	RMS of CL	St <sub>t1</sub>	St <sub>t2</sub>
210 × 153	10/3	2.410	0.589	-1.275	0.786	0.160	0.173
210 × 153	3.6	2.416	0.559	-1.276	0.761	0.173	0.173
210 × 193	3.6	2.492	0.594	-1.353	0.815	0.180	0.180
For SC II							
Grid	$\Delta t \times 10^3$	CD	RMS of CD	CL	RMS of CL	St <sub>t1</sub>	St <sub>t2</sub>
210 × 153	10/3	1.957	0.369	-0.113	0.680	0.073	0.160
210 × 153	3.6	1.890	0.300	-0.173	0.607	0.08	0.173
210 × 193	3.6	1.899	0.342	-0.155	0.678	0.08	0.173

coefficients of the scheme:

$$B = \frac{s_3^3 - s_2^3}{h_i \Delta}, \quad C = -\frac{s_2^2 - s_3^3}{h_i \Delta}, \quad A = -Bs_2^2 - Cs_3^2 \quad (14)$$

$$D = \begin{cases} (Ah_i^4 + B(h_i + h_{i-1})^4 + Ch_{i+1}^4)/24 & \text{for } u_{ij} > 0 \\ 0 & \text{otherwise} \end{cases} \quad (15)$$

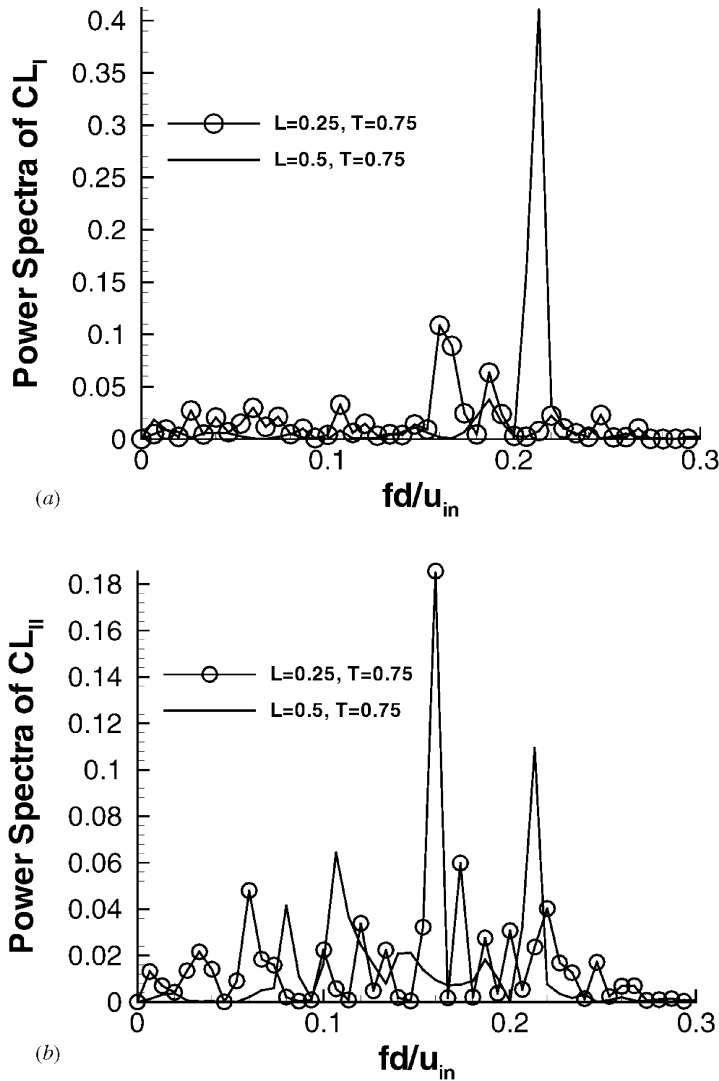


**Figure 3.** Power spectra of the coefficients of lift ( $CL$ ) plotted as functions of frequency for two cases of cylinder spacing for (a) the lift on SC I and (b) the lift on SC II. The power spectrum was evaluated from the temporal sequence of lift coefficient with time ranging from 50 to 200.

where  $s_2 = (h_{i-1} + h_i)/h_i$ ,  $s_3 = h_{i+1}/h_i$ , and  $\Delta = s_2 s_3 (s_2 - 1)(s_3 + 1)(s_2 + s_3)$ . Clearly, the upwind scheme expressed by Eq. (13) has fourth-order accuracy in discretization when  $u_{ij}$  is positive, and has third-order accuracy in discretization when is negative, since the coefficients ( $A, B, C$ ) have order  $O(1/h_i)$ . Similar expressions can be derived for the upwind differencing of other convective terms. The fourth-order derivative of  $u$  in Eq. (13) can be discretized by the central difference approach, which is used for treating the diffusion terms in the governing equations.

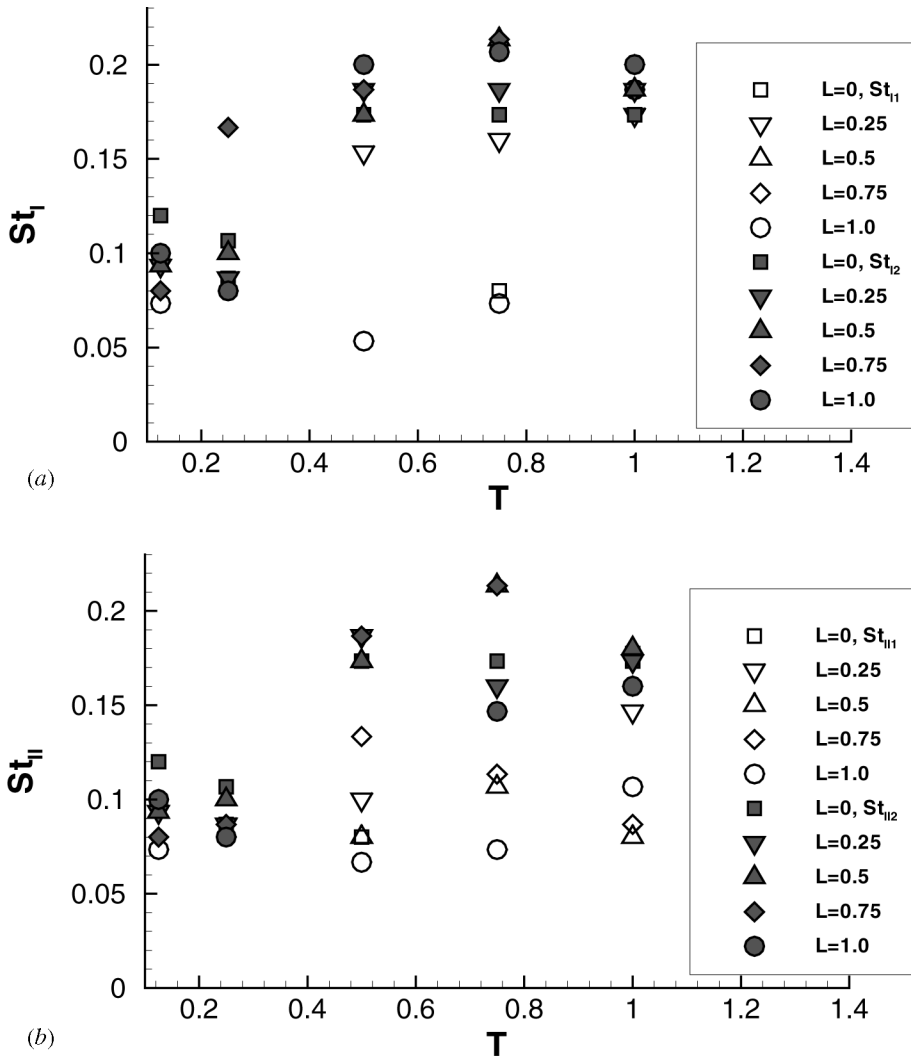


**Figure 4.** Strouhal number versus transverse spacing in the case of various longitudinal spacings for vortex shedding from the shear layers of SC I (a) and SC II (b).  $St_{I1}$  and  $St_{II1}$  are labeled by nonfilled symbols and are relevant to the vortex shedding from the outer shear flow layers of the two identical SC;  $St_{I2}$  and  $St_{II2}$  are labeled by filled symbols and correspond to the vortex shedding from the inner shear layers of the TISC.

The criterion for convergence in the pressure calculation is that the grid-number-averaged global residual is as low as  $3.0 \times 10^{-8}$ . The advantage of this joint method for pressure estimation is that it has higher accuracy than the AF1 method alone [24].

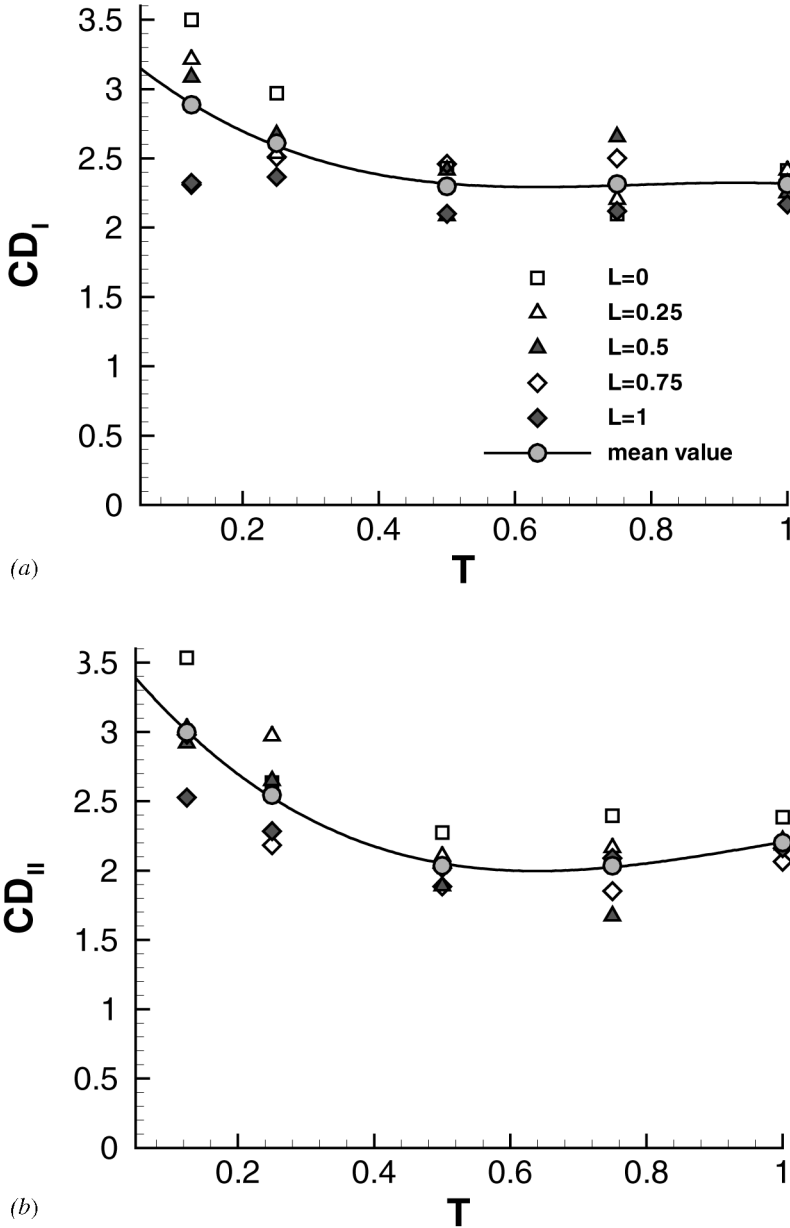


**Figure 5.** Time-averaged (mean) coefficients of drag on SC I (a) and SC II (b), plotted as functions of transverse spacing in the case of various longitudinal spacings. Note that the labels of symbols in (b) are the same as in (a). The mean value was evaluated from results of the six cases characterized by longitudinal spacing.

The Bi-CGSTAB has been used alone for the pressure field prediction [25]. However, it needs many more steps to obtain the pressure field. In the Bi-CGSTAB method, for the convenience of code construction, a Jacobian-type preconditioner is used, since the SSOR-type preconditioner given by Pennacchio and Simoncini [26] is more complex in simulator coding, even though it was reported that the SSOR-type preconditioner has almost the best performance.

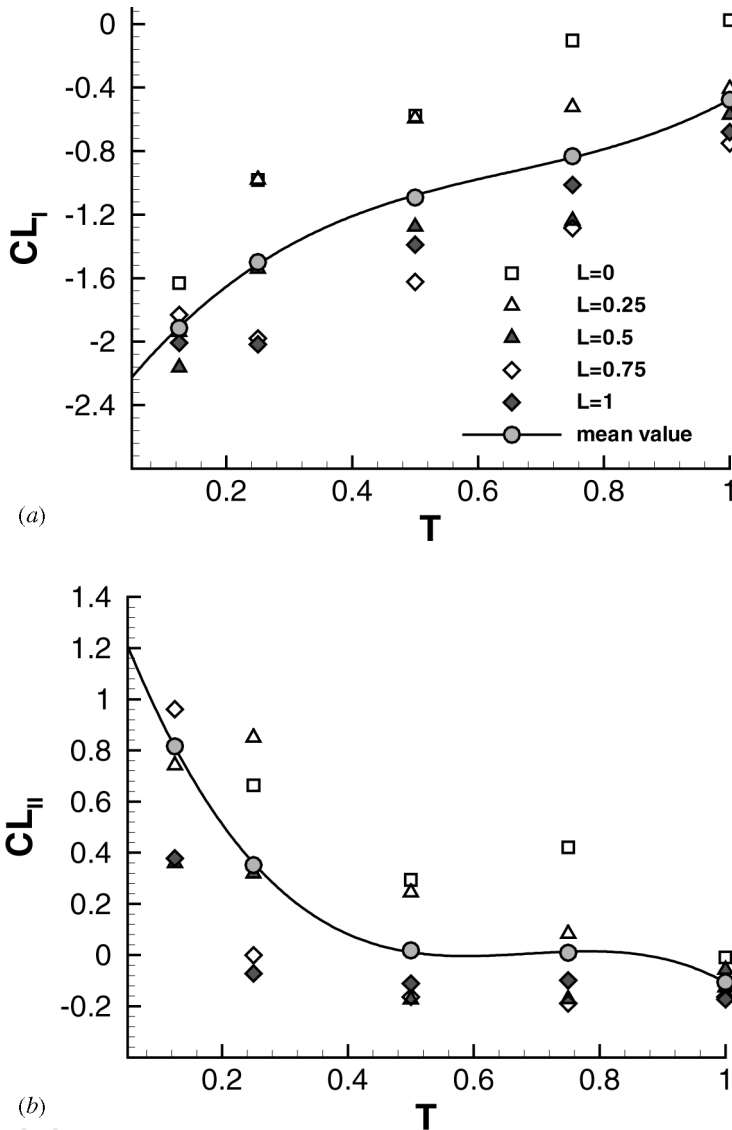


**Figure 6.** Time-averaged (mean) coefficients of lifts on SC I (a) and SC II (b), plotted as functions of transverse spacing in the case of various longitudinal spacings.

### 2.3. Method Assessment and Grid Independence Inspection

The numerical method given above was assessed by comparing the Strouhal number and the mean coefficient of drag (CD) of the wake flow around a single square cylinder with published data for the case of Reynolds number 250. For single square cylinder (SC) wake flow, at  $Re = 250$ , as numerical work of Sohankar et al. [11] has shown, the Strouhal number,  $St$ , is about 0.150 in the case of a given blockage value of 5.56%, while results in the past decade [10] suggest a Strouhal number of 0.142. Using the previously mentioned numerical method, with grid number  $181 \times 121$  and time step 0.005, it was found that the relevant  $St$  value is 0.140 from the evolution of flow-induced forces given in Figure 2. This suggests that the present method can predict the vortex shedding frequency in good agreement with published values.

On the other hand, at  $Re = 250$ , the mean coefficient of drag (CD) calculated by Saha et al. [10] for single SC wake flow is about 1.70 at the blockage of 10%; the work of Sohankar et al. [11] shows that the CD should be 1.49 at the blockage of 5.56%. For the same blockage (5.56%), the present calculation gives rise to a CD value of 1.79, indicating that the code used in the simulation can output mean drag in good consistency with those published but obtained by different numerical methods. Note that at  $Re = 250$ , the single-cylinder wake flow has a three-dimensional property, which may be the feature causing the discrepancy of flow simulation. This will be discussed elsewhere.

The grid independence inspection was carried out prior to extensive numerical simulation for  $T = L = 0.5$ . The computational domain (see Figure 1) was chosen so that the distance from the inlet section to the front side of the upstream SC is  $H_{xu} (= 8.5)$ , with the same value as the distance from the SC side wall to the side boundary of the computation domain, indicating that  $H_{yu} = H_{xu}$ . The distance from the rear side of the downstream SC II to the flow outlet section is 15, and the blockage of the flow in the present calculation can be expressed as  $1/(1 + 0.5T + 8.5)$ , with  $T$  representing the transverse spacing.

The smallest mesh size near a SC wall is approximately equal to 0.01. There are 20 grids on each side of the square cylinder. Smaller mesh size was assigned at the cylinder corner regions because flow separation inevitably results in greater pressure gradients in these regions. It is shown in Table 1 that the effects of grid change on the mean drag and lift coefficients as well as on  $St$  are negligible.

**Table 2.** Coefficients of polynomial fitting by  $T$  for aerodynamic parameters<sup>a</sup>

$\Phi$	$a_0$	$a_1$	$a_2$	$a_3$
CD <sub>I</sub>	3.352	-4.333	5.762	-2.464
CD <sub>II</sub>	3.686	-6.328	7.391	-2.545
CL <sub>I</sub>	-2.474	5.326	-6.810	3.483
CL <sub>II</sub>	1.532	-6.969	10.379	-5.048
RMS of CD <sub>I</sub>	0.676	-0.529	0.566	-0.204
RMS of CD <sub>II</sub>	0.652	-0.773	0.591	-0.049
RMS of CL <sub>I</sub>	1.430	-4.315	6.930	-3.132
RMS of CL <sub>II</sub>	2.321	-6.938	8.980	-3.278

<sup>a</sup>Available for  $T$  ranging from 0.125 to 1.0.  $\Phi = \sum_0^3 a_i T^i$ .

### 3. RESULTS AND DISCUSSION

The flow past the TISC is naturally transient at  $Re = 250$ , owing to the presence of the spanwise vortex structures which play an important role in decreasing the temporal oscillating magnitudes of the aerodynamic forces, but generally without apparent impact on the time-averaged value of the forces. This means that for the wake flow at  $Re = 250$ , a 2-D Navier-Stokes (NS) model can provide reasonable time-averaged results. Alternatively, a 3-D NS model should be applied to achieve more accurate solution of the oscillation-related features, and this will be carried

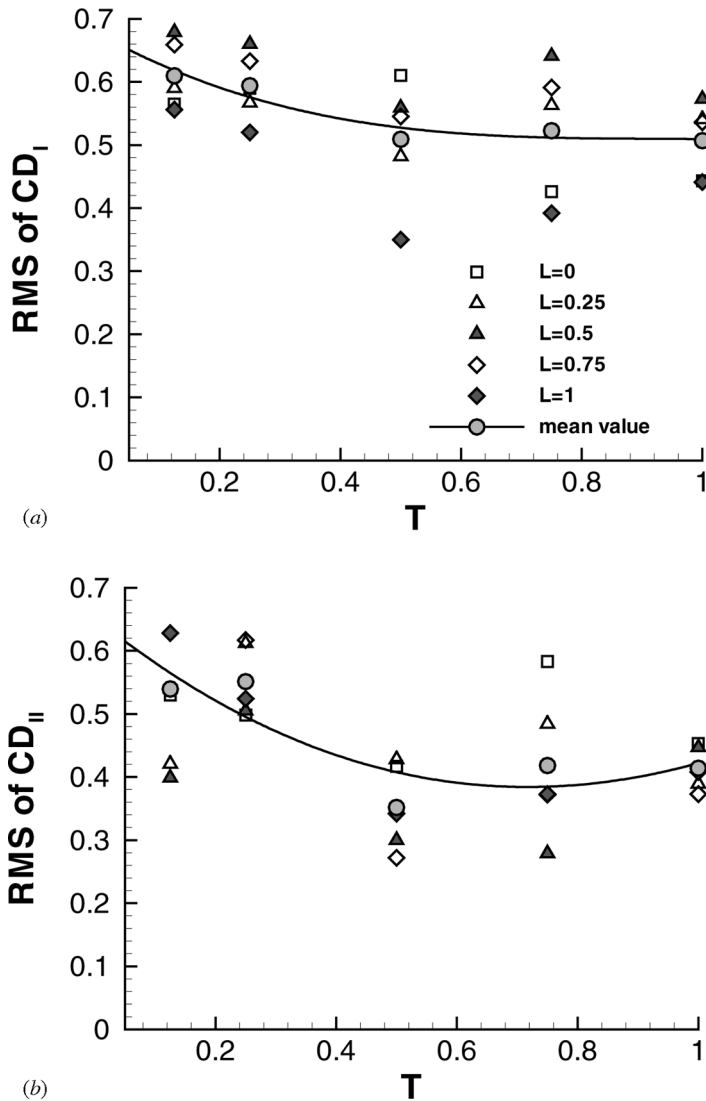


**Figure 7.** RMS of the coefficients of drag on SC I (a) and SC II (b), plotted as functions of transverse spacing in the case of various longitudinal spacings.

out in further work in near future. The remainder of this section describes the simulation results for the aerodynamic forces, convective heat transfer, and the vorticity and temperature fields.

### 3.1. Flow-Induced Forces

The flow-induced forces acting on a TISC arranged in close proximity are transient and are usually measured by the normalized primary frequencies of force oscillations (defined as the Strouhal number,  $St$ ), the mean (time-averaged)

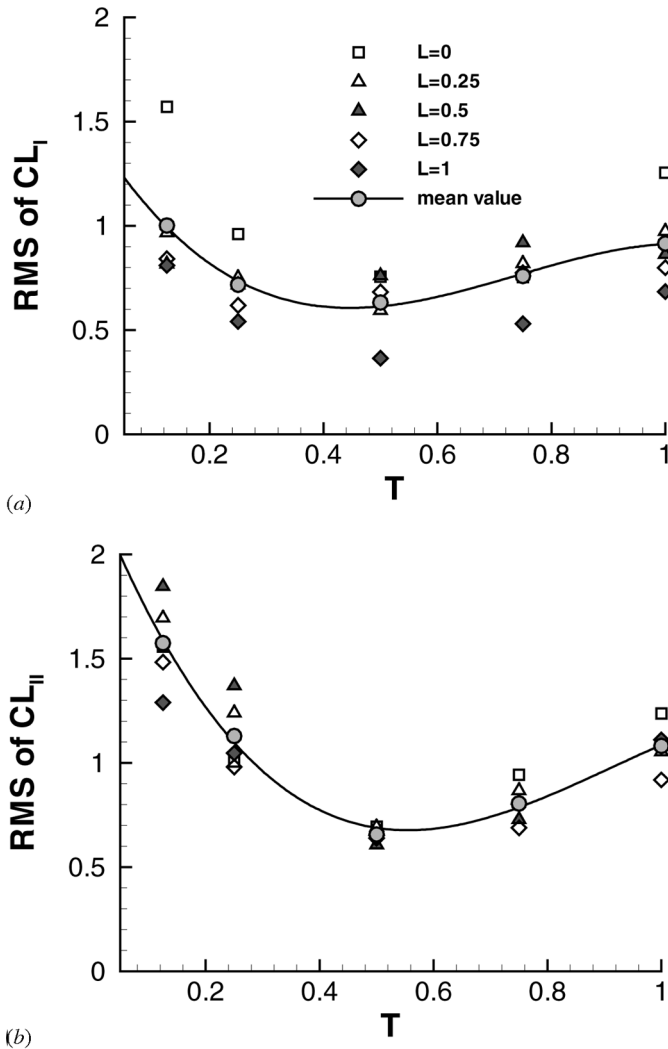


**Figure 8.** RMS of the coefficients of lift on SC I (a) and SC II (b), plotted as functions of transverse spacing in the case of various longitudinal spacings.

coefficients of drag (CD) and lift (CL) and their relevant root-mean-square (RMS) values. The Strouhal numbers were evaluated from the corresponding power spectra, where were in turn obtained by performing discrete Hilbert transformation [27] of the temporal data sequences of CL for the time range from 50 to 200. For instance, for the case of  $L = 0.25$ , and  $T = 0.75$ , the two pulses of power spectra shown in Figure 3a suggest that  $St_{I1} = 0.160$ ,  $St_{I2} = 0.187$ , with the similar two power-spectrum pulses in Figure 3b illustrating that  $St_{III1} = St_{III2} = 0.160$ . For the case of  $L = 0.5$ ,  $T = 0.75$ , it can be found that  $St_{I1} = St_{I2} = 0.213$  from Figure 3a, and  $St_{III1} = 0.107$ ,  $St_{III2} = 0.213$ . Here the Strouhal numbers  $St_{I1}$ ,  $St_{I2}$  correspond to the vortex shedding frequencies from the outer and inner shear layers of the bottom square cylinder, while  $St_{III1}$  and  $St_{III2}$  are relevant to the vortex shedding frequencies from the outer and inner shear layers of the top square cylinder.

The duplicate values of St reflect that, for a given value of longitudinal spacing, the St-T diagram (Figure 4) might show a bifurcation, indicating that the TISC arrangement effect on St is dominant. The St bifurcation as shown in Figure 4 implies that there is interaction between vortices shed with different periods in the vortex street of TISC. Such vortex interaction not only influences the flow-induced forces and wake flow patterns but also affects the convective heat transfer from the TISC.

To evaluate the variation tendencies of CD and CL and their RMS values with the transverse spacing, the 25 cases considered were divided into five groups with

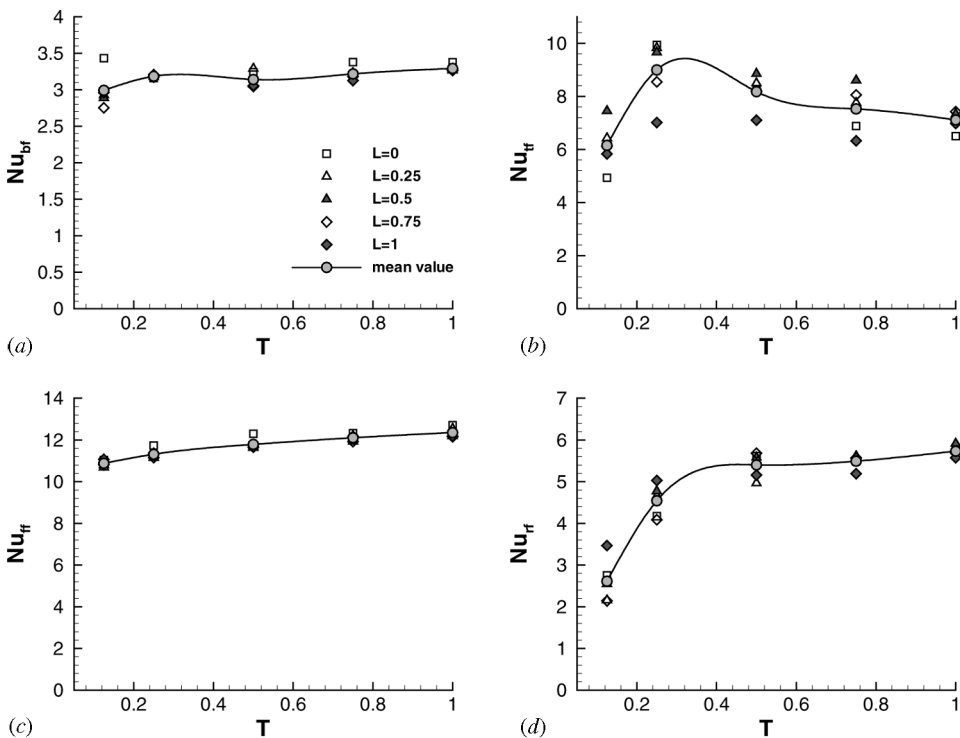


**Figure 9.** Time-averaged face Nusselt numbers for SC I plotted as functions of transverse spacing in the case of various longitudinal spacings on the (a) bottom, (b) top, (c) front, and (d) rear faces.

respect to the value of transverse spacing. Each group contains six particular cases labeled by the longitudinal spacing, whose values are given by  $L = 0, 0.25, 0.5, 0.75,$  and  $1.0,$  respectively. The mean value within each group was obtained by arithmetic averaging. The mean coefficients of drags ( $CD_I, CD_{II}$ ) of the flow around the TISC were shown in Figures 5a and 5b, with the mean coefficients of lifts ( $CL_I, CL_{II}$ ) given in Figures 6a and 6b. It is seen that the mean coefficients of drag decrease almost linearly as the transverse spacing starts to increase from 0.125 to about 0.4. On the other hand, the mean coefficient of drag  $CD_I$  is almost a constant of 2.4, with a constant 2.1 for the mean coefficient of drag  $CD_{II}$ . It can be well fitted by the third-order polynomials for the variation tendencies of  $CD$  and  $CL$  as well as their RMS values with the transverse spacing  $T$ . The coefficients of polynomial fitting are shown in Table 2.

Generally, the bottom square cylinder (SC I) is subjected to a repulsive lift force owing to the existence of the top one. The repulsive lift force denoted by  $CL_I$  has a mean value of  $-1.91$  for the transverse spacing  $T = 0.125$ . Figure 6a indicates that the repulsive lift force averaged arithmetically within each group has an excellent third-order polynomial fitting, whose coefficients were given in the fourth row of Table 2. On the other hand, Figure 6b shows that a repulsive lift force is also imposed on the downstream square cylinder (SC II) when the transverse spacing is smaller than 0.5. For cases of longitudinal spacing ranging from 0.5 to

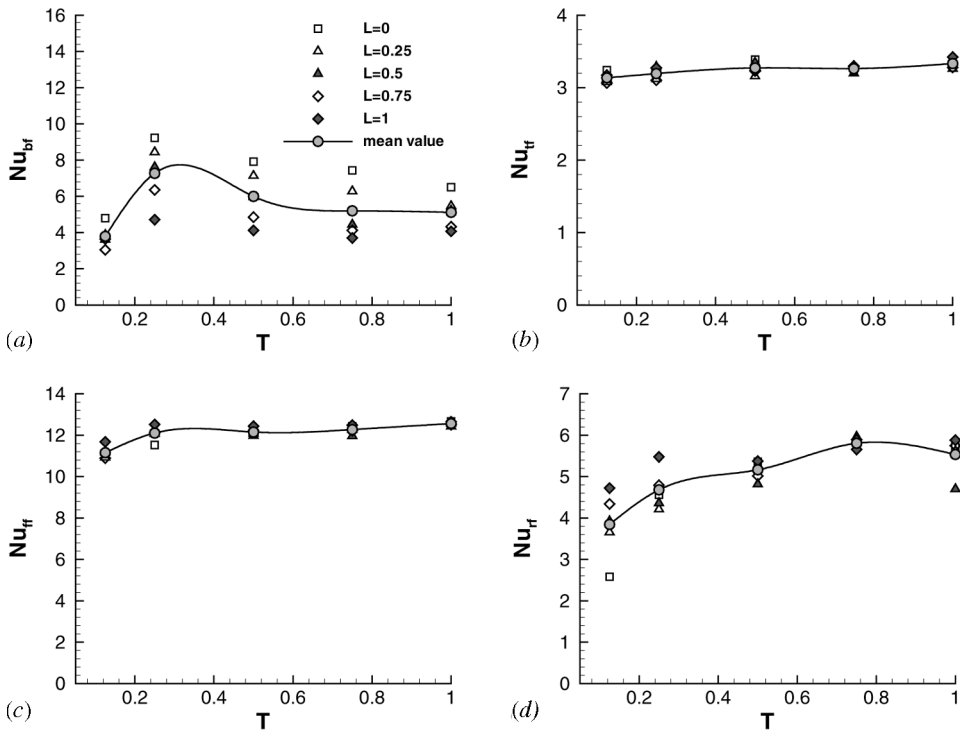


**Figure 10.** Time-averaged face Nusselt numbers for SC II plotted as functions of transverse spacing in the case of various longitudinal spacings on the (a) bottom, (b) top, (c) front, and (d) rear faces.

1.0, an attractive lift force on SC II occurs when the transverse spacing takes a value in the range from 0.5 to 1.0, showing that the lifts are very sensitive to the proximity arrangement of the two identical square cylinders.

As shown in Figures 7 and 8, the RMS of drags and lifts on the TISC varies with the transverse spacing in a similar way: decreasing quickly for small transverse spacing at first, reaching their minima and then growing gradually with the transverse spacing. The data for the mean value within each group for RMS of CD and CL can also be well fitted by polynomials. As illustrated in Figure 8, comparison between the two parts of Figure 8 shows that the RMS of lift on SC II is significantly greater than that on the upstream SC I when the transverse spacing is less than or equal to 0.25, while they are close to each other when the transverse spacing ranges from 0.5 to 1.0. It is noted that these RMS values should be qualitatively reasonable, since they are obtained by 2-D flow simulation. For the case of square cylinder flow at  $Re = 250$ , the actually existing secondary flow can decrease the oscillating magnitude of lift significantly.

### 3.2. Nusselt Numbers

Figures 9 and 10 show plots of the time-averaged face Nusselt numbers as functions of transverse spacing, with the span of data scatter for a particular transverse

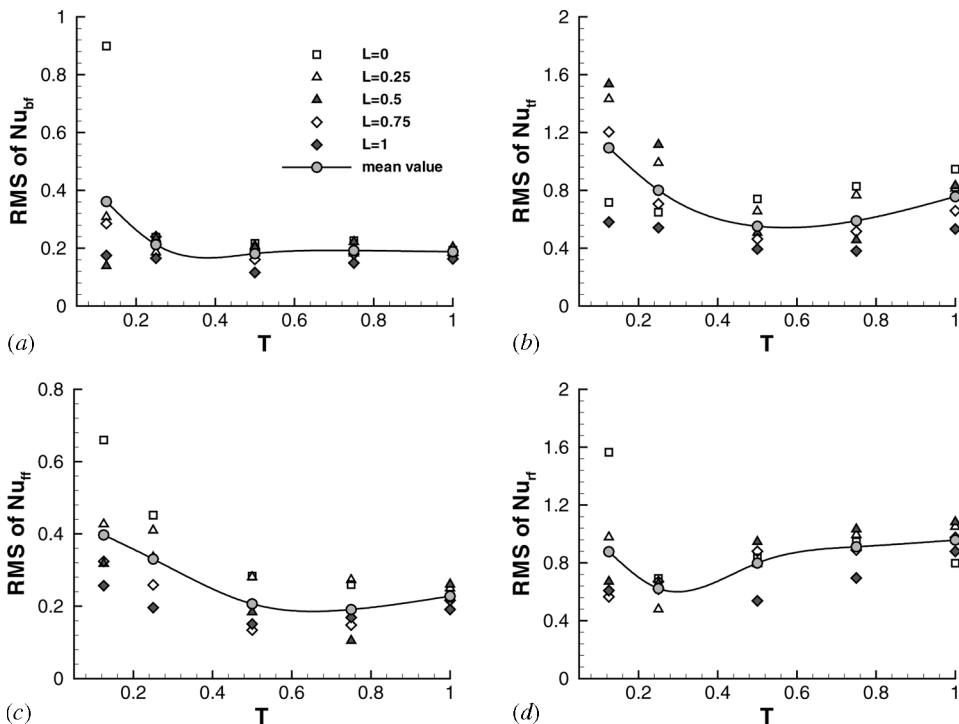


**Figure 11.** RMS of face Nusselt numbers for SC I plotted as functions of transverse spacing in the case of various longitudinal spacings on the (a) bottom, (b) top, (c) front, and (d) rear faces.

spacing indicating the relevant influence of longitudinal spacing. With a maximum discrepancy of about 10%, the mean Nusselt numbers on the outer faces of the TISC are close to a constant 3.2; while the mean Nusselt number on the front face is approximately close to 11.8, as depicted by Figures 9a and 9c, and Figures 10b and 10c. This implies that the mean face Nusselt numbers are almost insensitive to the change of transverse spacing. The shortest span of data scattering at a given transverse spacing for the mean Nusselt numbers on the front and outer faces suggests that influence from the change of the longitudinal spacing is almost negligible.

However, the mean Nusselt numbers on the rear and inner faces of the TISC depend evidently on the transverse and longitudinal spacing values. For the mean value within each group, the relevant curves based on spline-fitting (Figures 9b and 10a) show that the mean value within each group for the face Nusselt numbers on the inner sides of the TISC reaches a maximum when the transverse spacing is about 0.3. For larger transverse spacing ( $T \geq 0.5$ ), the mean value within each group for the face Nusselt number on the top face of SC I is about 7.5, with that on the bottom face of SC II approximately a constant value of 5.5, indicating that the mean Nusselt numbers on the inner faces are about 2 to 3 times those on the outer faces of the TISC.

For the case of  $T = 0.125$ , the effect of the longitudinal spacing is apparent in the RMS of the face Nusselt number. Similar to the dependence of the mean face Nusselt numbers on the TISC arrangement, as shown in Figures 11a and 11c, and

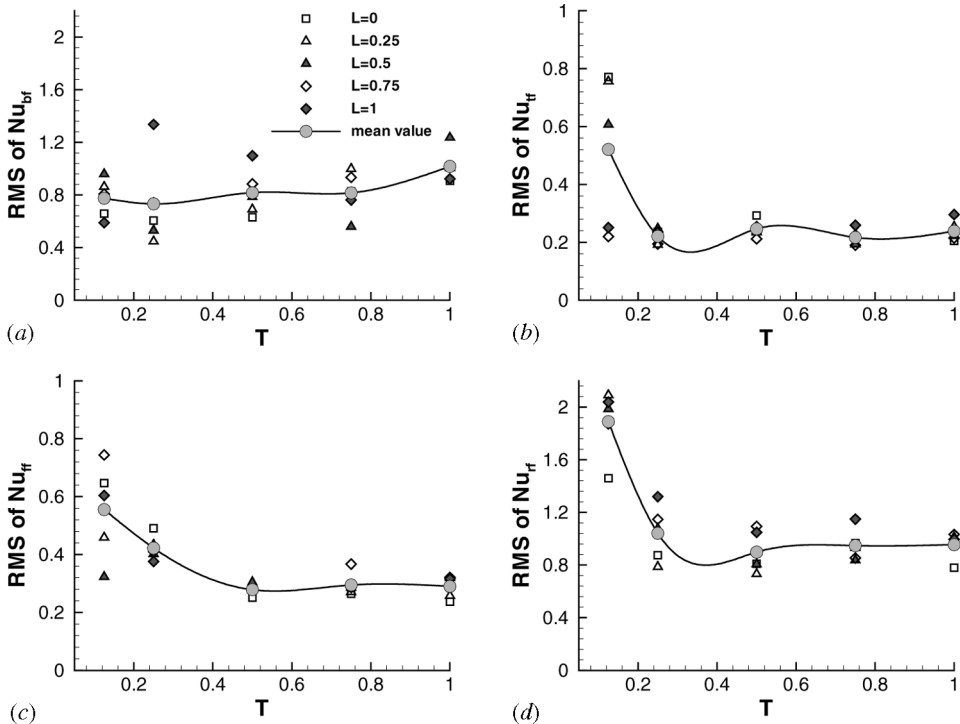
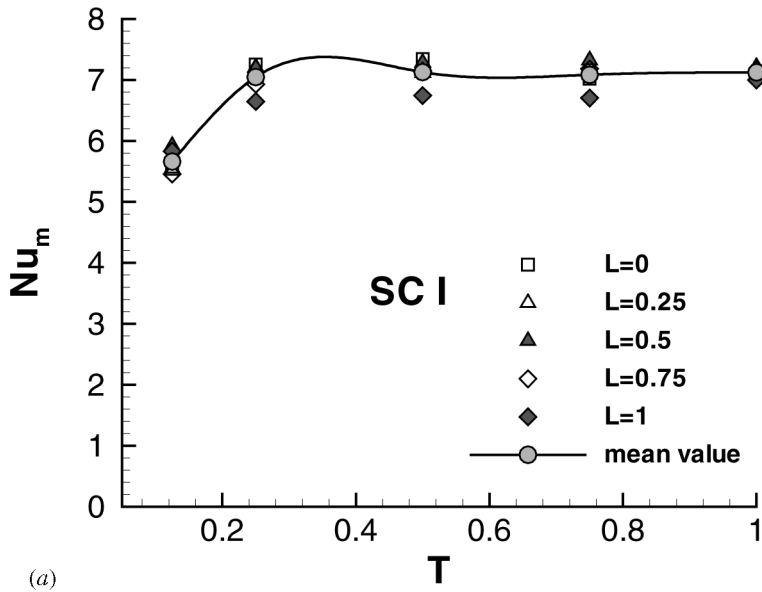
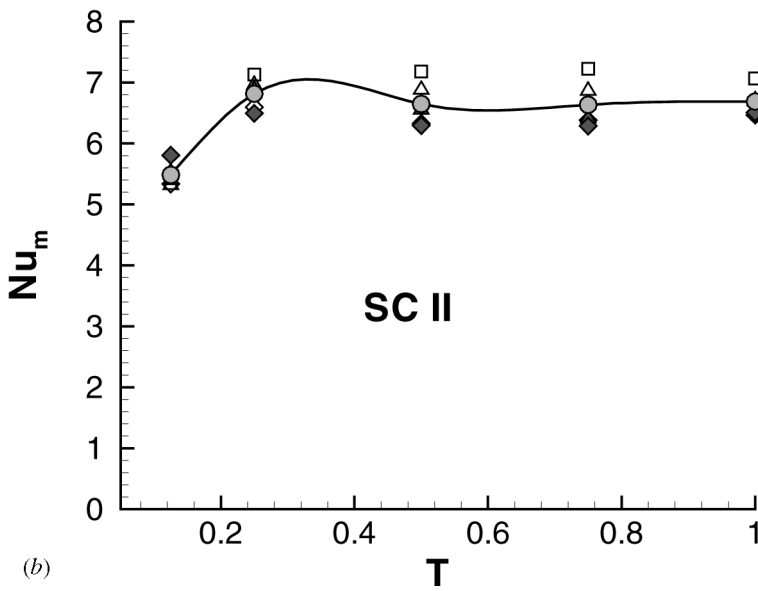


**Figure 12.** RMS of face Nusselt numbers for SC II plotted as functions of transverse spacing in the case of various longitudinal spacings on the (a) bottom, (b) top, (c) front, and (d) rear faces.



(a)



(b)

**Figure 13.** Time-averaged (mean) Nusselt number plotted as a function of transverse spacing in the case of various longitudinal spacings for (a) SC I and (b) SC II.

Figures 12b and 12c, the RMS of the Nusselt numbers on the front and outer faces of the TISC are smaller. In contrast, the RMS of the Nusselt numbers on the rear and inner faces of the TISC are larger and significantly sensitive to the transverse and the longitudinal spacing values.

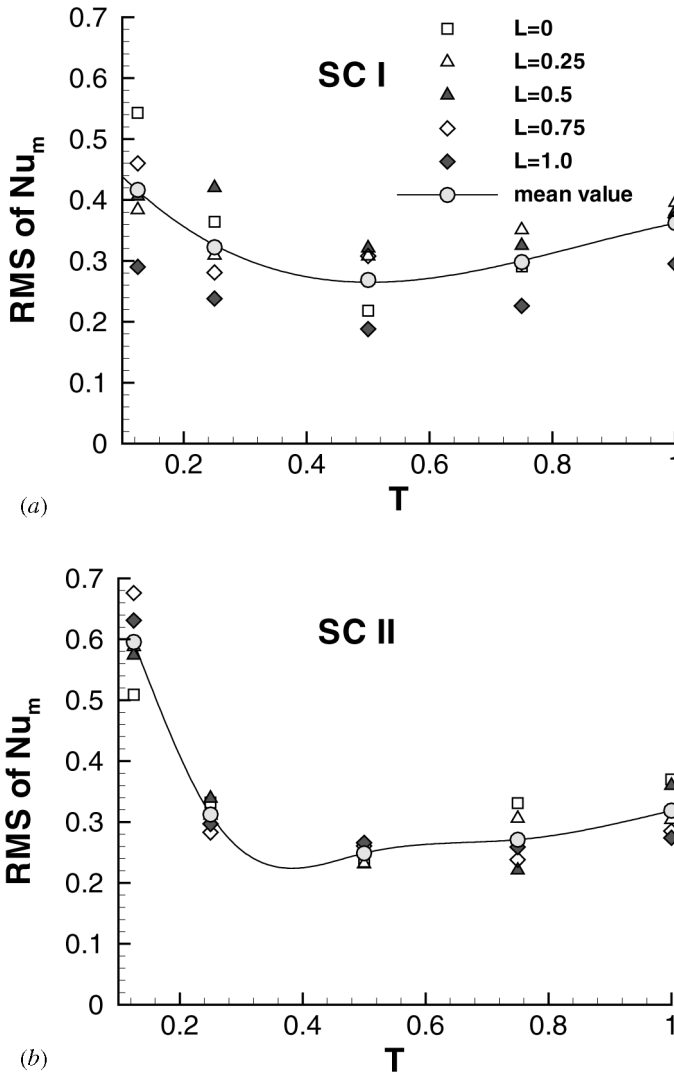


**Figure 14.** RMS of mean Nusselt number plotted as a function of transverse spacing in the case of various longitudinal spacings for (a) SC I and (b) SC II.

The time-average (mean) Nusselt numbers for the TISC have been plotted as functions of the transverse spacing in Figure 13. For the transverse spacing ranging from 0.25 to 1.0, the mean Nusselt number for the bottom square cylinder is about 7.1, with a value of 6.7 for the mean Nusselt number for the top square cylinder. For  $T = 0.125$ , the mean Nusselt number for the TISC takes a smaller value of about 5.5; this may be caused by the suppression of vortex shedding from the inner sides of the TISC due to the smaller transverse spacing. The maximum is likely to occur at  $T = 0.3$ . Furthermore, as shown in Figure 14, the RMS of the Nusselt numbers for the TISC are of the same order, and range from 0.25 to 0.7.

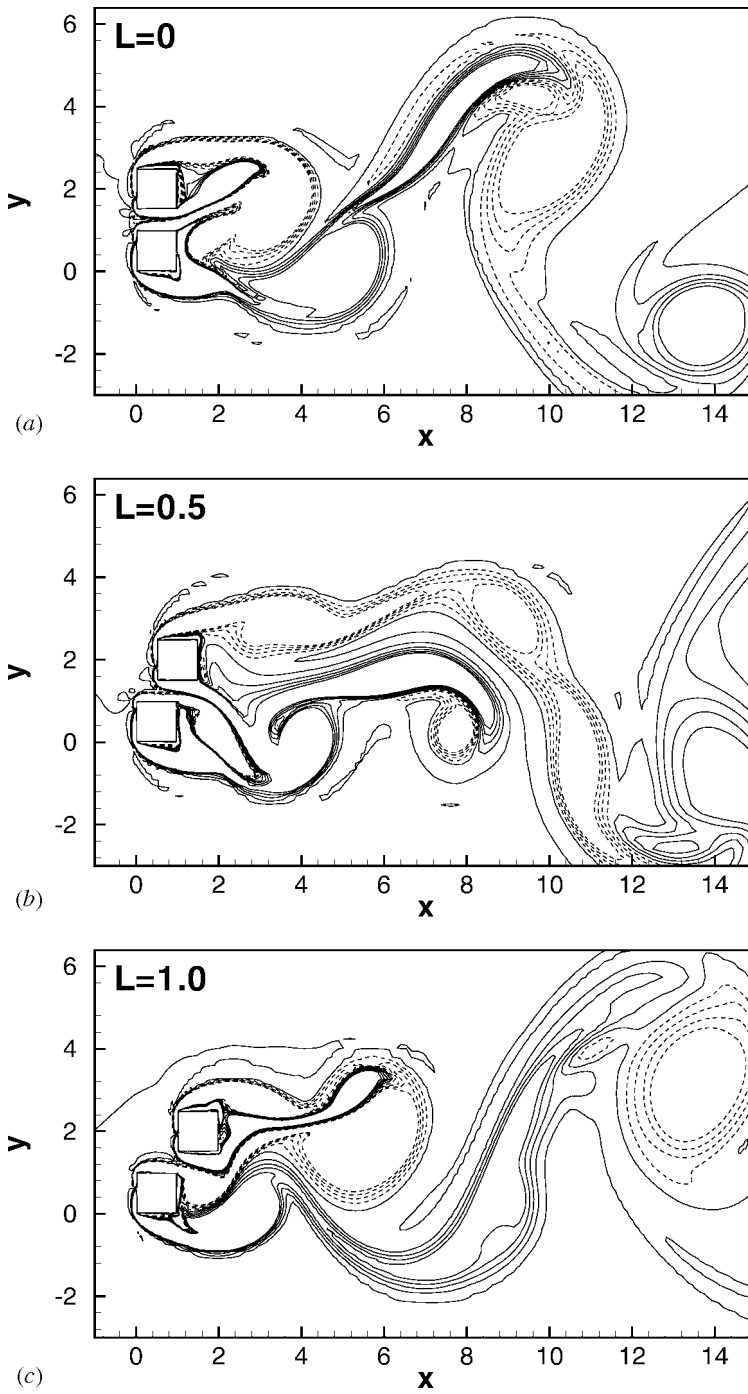


**Figure 15.** Vorticity fields at the instant  $t = 200$  for the case of  $T = 0.5$  at three different longitudinal spacings: (a)  $L = 0$ ; (b)  $L = 0.5$ ; (c)  $L = 1.0$ .

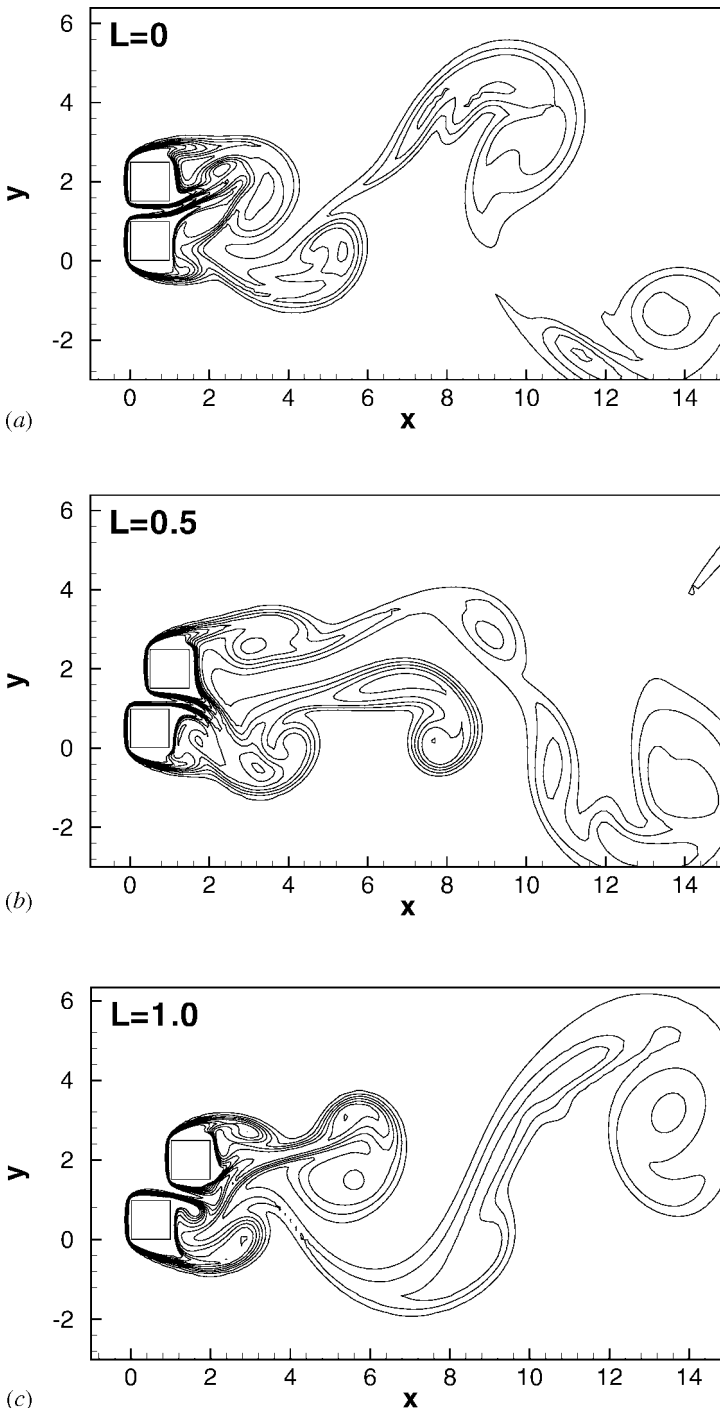


**Figure 16.** Temperature fields at the instant  $t = 200$  for the case of  $T = 0.5$  at three different longitudinal spacings: (a)  $L = 0$ ; (b)  $L = 0.5$ ; (c)  $L = 1.0$ .

### 3.3. Vorticity and Temperature Fields

The vorticity fields at the time of 200 for the case of  $T = 0.5$ , and  $L = 0, 0.5$ , and 1.0, are given in Figure 15. The clockwise vortices are illustrated by dashed lines, the vorticity values are labeled from  $-0.25$  to  $-1.0$  with an interval of 0.25; while the anticlockwise vortices are shown by solid lines, which are labeled by vorticity values from zero to 1.0 with an interval of 0.25. The flow patterns for the case of  $H = 0.5$  are characterized by vortex pairing, splitting, and enveloping patterns, as identified by Sumner et al. [28].

It is evident that the variation of the longitudinal spacing has caused significant changes in flow patterns. There exist the close proximity interference and the wake interference for the flow around the TISC. Clearly, these flow interferences are dominated by the TISC arrangement.

The relevant temperature fields are shown in Figure 16. The isotherm lines are labeled by the temperature values from 0.05 to 0.45 with an increment of 0.05. It is noted that the thermal cells occur corresponding to the presence of the large-scale vortices in the near-wake of the TISC.

## 4. CONCLUSIONS

The convective heat transfer from two identical square cylinders arranged in close proximity and submerged in a uniform cross flow at  $Re = 250$ ,  $Pr = 0.71$  has been studied numerically using a finite-difference method. The third-order upwind scheme was used to discretize the convective terms in the governing equations. This study emphasized the effect of the longitudinal spacing ranging from zero to unity, and the transverse spacing ranging from 0.125 to unity. The results of these extensive numerical experiments revealed that the time-averaged or mean convective heat transfer rates from the TISC at the particular Reynolds and Prandtl numbers are characterized by the transverse and longitudinal spacing values. The mean heat transfer rates from the inner faces are generally greater than those of the outer sides by a factor of approximately 2.0 to 3, owing mainly to the gap flow influence. Depending on the TISC arrangement, a bifurcation occurs in association with the Strouhal number for vortex shedding, with the bifurcated lower  $St$  value associated with the shedding from the outer shear layer, and the higher one associated with the shedding from the inner shear layer. Similarly, the effect of the TISC arrangement on the flow-induced forces is also significant. The mean Nusselt number on the TISC is about 7.0 for the transverse spacing in the range from 0.25 to unity, while it is about 5.5 for the transverse spacing of 0.125, due to the suppression of the vortex shedding in the inner sides of the TISC.

## REFERENCES

1. I. T. S. Yu, Y. Li, T. W. Wong, W. Tam, A. T. Chan, J. H. W. Lee, D. Y. C. Leung, and T. Ho, Evidence of Airborne Transmission of the Severe Acute Respiratory Syndrome Virus, *N. Engl. J. Med.*, vol. 350, pp. 1731–1739, 2004.
2. R. Hilpert, Wärmeabgabe von Geheiztem Drähten und Rohrem im Luftstrom, *Geb. Ingen.*, vol. 4–5, pp. 215–224, 1933.

3. M. Jacob, *Heat Transfer*, vol. 1, pp. 562–363, Wiley, New York, 1949.
4. I. Igarashi, Heat Transfer from a Square Prism to an Air Stream, *Int. J. Heat Mass Transfer*, vol. 28, pp. 175–181, 1985.
5. J. M. Chen and C. H. Liu, Vortex Shedding and Surface Pressures on a Square Cylinder at Incidence to a Uniform Air Stream, *Int. J. Heat Fluid Flow*, vol. 20, pp. 592–597, 1999.
6. T. Tamura and T. Myyagi, The Effect of Turbulence on Aerodynamic Forces on a Square Cylinder with Various Corner Shapes, *J. Wind Eng. Ind. Aerodyn.*, vol. 83, pp. 135–145, 1999.
7. C. K. Choi and D. K. Kwon, Effect of Corner Cuts and Angles of Attack on the Strouhal Number of Rectangular Cylinders, *Wind Struct.*, vol. 6, pp. 127–140, 2003.
8. S. C. Luo, Y. T. Chew, and Y. T. Ng, Characteristics of Square Cylinder Wake Transition Flows, *Phys. Fluids*, vol. 15, pp. 2549–2559, 2003.
9. R. W. Davis, E. F. Moore, and L. P. Purtell, A Numerical-Experimental Study on Confined Flow around Rectangular Cylinders, *Phys. Fluids*, vol. 23, pp. 46–59, 1984.
10. A. K. Saha, G. Biswas, and K. Muralidhar, Three-Dimensional Study of Flow past a Square Cylinder at Low Reynolds Numbers, *Int. J. Heat Fluid Flow*, vol. 24, pp. 54–66, 2003.
11. A. Sohankar, C. Norberg, and L. Davidson, Simulation of Three-Dimensional Flow around a Square Cylinder at Moderate Reynolds Numbers, *Phys. Fluids*, vol. 11, pp. 288–306, 1999.
12. J. L. Rosales, A. Ortega, and J. A. C. Humphrey, A Numerical Investigation of the Convective Heat Transfer in Unsteady Laminar Flow past a Single and Tandem Pair of Square Cylinders in a Channel, *Numer. Heat Transfer A*, vol. 38, pp. 443–465, 2000.
13. J. L. Rosales, A. Ortega, and J. A. C. Humphrey, A Numerical Simulation of the Convective Heat Transfer in a Confined Channel Flow past Square Cylinders: Comparison of Inline and Offset Tandem Pairs, *Int. J. Heat Mass Transfer*, vol. 44, pp. 587–603, 2001.
14. S. Turki, H. Abbassi, and S. B. Nasrallah, Two-Dimensional Laminar Fluid Flow and Heat Transfer in a Channel with a Built-in Heated Square Cylinder, *Int. J. Thermal Sci.*, vol. 42, pp. 1105–1113, 2003.
15. A. Sharma and V. Eswaran, Effect of Aiding and Opposing Buoyancy on the Heat and Fluid Flow across a Square Cylinder at  $RE = 100$ , *Numer. Heat Transfer A*, vol. 45 pp. 601–624, 2004.
16. A. Sharma and V. Eswaran, Heat and Fluid Flow across a Square Cylinder in the Two-Dimensional Laminar Flow Regime, *Numer. Heat Transfer A*, vol. 45, pp. 247–269, 2004.
17. A. Sharma and V. Eswaran, Effect of Channel Confinement on the Two-Dimensional Laminar Flow and Heat Transfer across a Square Cylinder, *Numer. Heat Transfer A*, vol. 47, pp. 79–107, 2005.
18. L. Yang and B. Farouk, Mixed Convention Around a Heated Rotating Horizontal Square Cylinder in a Circular Enclosure, *Numer. Heat Transfer A*, vol. 28, pp. 1–18, 1995.
19. Q. H. Wang and Y. Jaluria, Three-Dimensional Conjugate Heat Transfer in a Horizontal Channel with Discrete Heating, *J. Heat Transfer*, vol. 126, pp. 642–647, 2004.
20. I. Orlanski, A Simple Boundary Condition for Unbounded Flows, *J. Comput. Phys.*, vol. 21, pp. 251–269, 1976.
21. D. L. Brown, R. Cortez, and M. L. Minion, Accurate Projection Methods for the Incompressible Navier-Stokes Equations, *J. Comput. Phys.*, vol. 168, pp. 464–499, 2001.
22. T. J. Baker, Potential Flow Calculation by the Approximate Factorization Method, *J. Comput. Phys.*, vol. 42, pp. 1–19, 1981.
23. Von Der Vorst H., BiCGSTAB: A Fast and Smoothly Converging Variant of BICG for the Solution of Non-symmetric Linear System, SIAM, *J. Sci. Stat. Comput.*, vol. 13, pp. 631–644, 1992.

24. H. X. Yang and Z. J. Zhu, Exploring Super-critical Properties of Secondary Flows of Natural Convection in Inclined Channels, *Int. J. Heat Mass Transfer*, vol. 47, pp. 1217–1226, 2004.
25. H. X. Yang, Z. J. Zhu, and J. Gilleard, Numerical Simulation of Thermal Fluid Instability between Two Horizontal Parallel Plates, *Int. J. Heat Mass Transfer*, vol. 44, pp. 1485–1493, 2001.
26. M. Pennacchio and V. Simoncini, Efficient Algebraic Solution of Reaction-Diffusion System for Cardiac Excitation Process, *J. Comput. Appl. Math.*, vol. 145, pp. 49–70, 2002.
27. Z. J. Zhu and H. X. Yang, Discrete Hilbert Transformation and Its Application to Estimate the Wind Speed in Hong Kong, *J. Wind Eng. Ind. Aerodyn.*, vol. 90, pp. 9–18, 2002.
28. D. Sumner, S. J. Price, and M. P. Paidoussis, Flow-Pattern Identification for Two Staggered Circular Cylinders in Cross-flow, *J. Fluid Mech.*, vol. 411, pp. 263–303, 2000.